

# 1 Supplementary Information for

## 2 A New Approach to Characterizing the Partitioning of Volatile

### 3 Organic Compounds to Cotton Fabric

4 Jie Yu,<sup>1</sup> Frank Wania<sup>2</sup> and Jonathan P. D. Abbatt\*.<sup>1</sup>

5 <sup>1</sup>Department of Chemistry, University of Toronto, 80 St. George Street, Toronto, Ontario,  
6 M5S 3H6, Canada

7 <sup>2</sup>Department of Physical and Environmental Sciences, University of Toronto Scarborough,  
8 Toronto, 1265 Military Trail, Ontario, M1C 1A4, Canada

9 Email: jiejie.yu@utoronto.ca, frank.wania@utoronto.ca, jonathan.abbatt@utoronto.ca

#### 10 Table of Contents:

S1.	Vocus PTR-TOFMS operation	S2
S2.	VOC Calibration and PTR-TOFMS sensitivity	S2
S3.	Sample calculation: S3.1. Partition Ratio; S3.2. Surface Coverage	S4
S4.	Description of a long-term exposure in a Toronto apartment	S5
S5.	Justification on the variability of physicochemical properties of isomers	S6
Tab. S1	Saturated vapor pressure (VP) of liquid and log $K_{OA}$ for selected isomers.	S6
Fig. S1	Desorption time series for all compounds for February 2021 measurements.	S7
Fig. S2	Sample time series of ambient air concentration measurements for February 2021 measurements.	S8
Fig. S3	(A) Sample desorption time series of long-term exposure (2-10 weeks) in a Toronto apartment during May to July 2020; (B) corresponding desorption time series of the short-time exposure measured in laboratory during February 2021.	S9
Fig. S4	Demonstration of equilibration time: a plot of mass desorbed ( $\mu\text{g}$ ) from cotton fabrics with short-time (30 minute) thermal desorption with long-term exposure (2-10 weeks) for May to July 2020 measurements.	S10
Fig. S5	Evaluation of the short-time desorption data validity: $K_{CA, V}$ comparison for long-time (2 hour, February 2021 and December 2020 measurements) and short-time (30 minute, December 2020 measurements) thermal desorption times.	S11
Fig. S6	Time series of ambient temperature and relative humidity during exposure period in February 2021.	S12
Fig. S7	The comparison of surface adsorption partitioning ratio for ethylbenzene with ppLFER prediction and past measurement of other adsorption systems.	S12
Fig. S8	Illustrations for (A) Exposure set up; (B) Flow cell system.	S13
Tab. S2	(A) Calibration factor (CF) of calibrated VOCs and predicted $k_{\text{proton-transfer}}$ values; (B) Predicted calibration factors for all VOCs.	S14
Tab. S3	Summary of the numerical values of $K_{CA, V}$ and $K_{CA, S}$ , and log $K_{OA}$ values.	S15
	References	S16

## 12 **Supplementary Text and Figures**

### 13 **S1. Vocus PTR-TOFMS Operation**

14 The VOCs desorbed from cloth samples upon heating in the stainless-steel cell were measured  
15 with a Vocus PTR-TOFM (Aerodyne Research Inc.). With a focusing ion-molecule reactor  
16 (FIMR), the detection efficiency of ions is improved as compared to conventional PTR  
17 instruments.<sup>1</sup> A 1.2 m long flight tube in the time-of-flight (TOF) analyzer enhances the mass  
18 resolving power up to 12,000.<sup>1</sup>

19

20 From the stainless-steel cell, sample air was drawn into the Vocus inlet through a 50 cm long  
21 PFA Teflon tubing (ID 3.97 mm, OD 6.35 mm, wrapped with heating tape maintained at 55  
22 °C) at a flow rate of 600 cm<sup>3</sup>/minute. 100 cm<sup>3</sup>/minute of this flow was sampled into the Vocus,  
23 while the remainder passed to a KNF diaphragm pump (model UN911 KVP) to enhance the  
24 total flow. The Vocus operating conditions were as follows:

- 25 (i) reagent ions (H<sub>3</sub>O<sup>+</sup>) produced in the discharge ion source originated from HPLC-grade  
26 milli-Q water at 105 Pa and 273.15 K, at a flow rate of 20 cm<sup>3</sup>/minute;
- 27 (ii) the focusing ion–molecule reactor (FIRM) was operated at a pressure of 220 Pascal;
- 28 (iii) discharge voltage: 425 V; discharge voltage current: 2 mA; E/N = 79 Td.

29 For measurements of thermal desorption and ambient air during exposure period, raw data were  
30 recorded with a time resolution of 10 seconds and 10 minutes, respectively. Tofware software  
31 (version 3.2.2) was used for analysis.

32

### 33 **S2. VOC Calibration and PTR-TOFMS sensitivity**

34 A “syringe pump” approach described in Liu and Abbatt (2021) was used to calibrate selected  
35 VOCs from the 3 homologous series.<sup>2</sup> The calibration was performed under dry conditions (0%  
36 RH), as the experimental RH condition was low and literature has demonstrated little RH  
37 impact on VOC sensitivities within the RH range of 0–60%.<sup>1,2</sup> C9 carbonyl-Nonanal, C4  
38 carboxylic acid-butanoic acid, C4 carboxylic acid-hexanoic acid, C7 aromatic-toluene (all from  
39 Sigma-Aldrich) and C2 carboxylic acid-acetic acid (Fisher Scientific) were calibrated. The  
40 fractions of parent ion to fragment ion(s) fragmentation were calculated for predicting the  
41 sensitivity calibration factors (CFs) of the remainder VOCs of the same chemical class  
42 category. Table S3 (A) summarizes the sensitivities of calibrated VOCs.

43

44 The sensitivity calibration factors (CFs; unit of counts per second per parts per billion, or  
45 cps/ppb) of the remaining VOCs were predicted based on the proton-transfer reaction rate  
46 coefficients ( $k_{\text{proton-transfer}}$ ; cm<sup>3</sup>/ (molecule · s)). The  $k_{\text{proton-transfer}}$  values for all VOCs can be

47 predicted from the approach proposed by Sekimoto et al., which is based on the polarizability  
48 ( $\alpha$ ;  $\text{cm}^3$ ) and dipole moment ( $\mu$ ; D) of the targeted chemicals.<sup>3</sup> Similar to previous literature  
49 findings, the sensitivities of calibrated VOCs (corrected for fragmentation) correlates linearly  
50 with  $k_{\text{proton-transfer}}$ .<sup>1,2</sup>

51

$$52 \quad \text{Sensitivity Calibration Factor (cps/ppb)} = 6.0 \times 10^{11} \cdot k_{\text{proton-transfer}} \quad (1)$$

53

54 The set of sensitivity data used is a combination of VOCs calibrated in this study and in Liu  
55 and Abbatt (2021), as both calibrations were operated with the same instrument and parameters.

56 <sup>2</sup> The  $k_{\text{proton-transfer}}$  values for calibrated VOCs are obtained from an online publicly available  
57 library of proton-transfer reactions with  $\text{H}_3\text{O}^+$  ions by Pagonis et al. (2019) and are listed in  
58 Table S3 (A).<sup>4</sup> The coefficient  $6.0 \times 10^{11}$  in equation (1) is obtained from the fitted linear  
59 equation of this set of sensitivity and  $k_{\text{proton-transfer}}$  data. As a result, by combining the estimated  
60  $k_{\text{proton-transfer}}$  and the sensitivity- $k_{\text{proton-transfer}}$  correlation shown in equation (1), the sensitivity of  
61 the remainder VOCs can be predicted. The parent ion sensitivity can be obtained assuming the  
62 parent ion fraction is the same as the calibrated VOC from that homologous series (carbonyl,  
63 carboxylic or aromatics). Table S3 (B) lists the predicted sensitivities for all VOCs and the  
64 relevant parameters.

65

66 Due to the BSQ (big segmented quadrupole) bandpass properties in the Vocus, a VOC with  
67 molecular weight below 58 has an ion transmission efficiency  $< 100\%$ .<sup>1</sup> For VOCs in this study,  
68 C1 carboxylic acid (ie. formic acid) is the only one with molecular weight below 58, Krechmer  
69 et al. obtained a transmission efficiency of 50%. This low transmission efficiency was taken  
70 into account in the sensitivity prediction.<sup>1</sup>

### 71 S3. Sample Calculations

#### 72 S3.1. Partition ratio

73 Example for C3 Carbonyl

74 **Known:** Sensitivity calibration factor (CF) = 234 cps/ppb; Area under desorption time series (A) = 1.1  
75  $\times 10^7$  cps  $\times$  s; 1 ppb =  $2.46 \times 10^{10}$  molecules/cm<sup>3</sup> at 298 K and 1 atm; flow rate = 600 cm<sup>3</sup>/min; Mass  
76 of cloth piece = 0.2 g; Molecular weight = 58.08 g/mol; Density of cotton cloth = 1.5 g/cm<sup>3</sup>; Average  
77 PTR-MS signal during air sampling ( $S_{avg}$ ) = 2411 cps; Average gas-phase concentration ( $C_{mr,air}$ ) =  
78  $S_{avg} / CF = 2411 \text{ cps} / (234 \text{ cps/ppb}) = 10.4 \text{ ppb}$ , i.e.  $C_{conc,air} = 24.5 \text{ ug/m}^3$ . [Note that this calculation  
79 assumes that the ambient from the heated cotton has returned close to room temperature (assumed to be  
80 298 K) by the time it is sampled by the PTR-MS. While the flow might be somewhat hotter than true  
81 room temperature, there errors associated with this assumption are minor, well less than 10%.]

82 **Method:**

$$83 \text{ Log } K_{CA\_V} = \log \frac{\frac{m_{desorbed}}{V_{cloth}}}{C_{conc,air}} = \log \frac{\frac{A \times F}{CF}}{\frac{V_{cloth} S_{avg}}{CF}} = \log \frac{A \times F}{V_{cloth} S_{avg}} = \log \frac{(1.1 \times 10^7 \text{ cps} \times \text{s}) \times (\frac{600 \text{ cm}^3}{\text{min}} \times \frac{1 \text{ min}}{60 \text{ s}})}{1.33 \times 10^{-7} \text{ m}^3 \times 2411 \text{ cps}} = 5.53$$

84 ( $\mu\text{g/m}^3$  of cloth) / ( $\mu\text{g/m}^3$  of air)

85 where F = flow of air over the cotton. Since  $K_{CA\_V} = K_{CA\_S} \times (SA_{cloth}/V_{cloth})$ , and  $SA_{cloth}/V_{cloth} =$   
86  $4.8 \times 10^5 \text{ m}^{-1}$  for this cloth sample specifically,  $\log K_{CA\_S} = -0.161$  ( $\mu\text{g/m}^2$  of cloth) / ( $\mu\text{g/m}^3$   
87 of air).

88

#### 89 S3.2. Surface coverage

90 Example for C3 Carbonyl

91 **Known:** Specific Surface area = 0.32 m<sup>2</sup>/g; Mass of cloth piece = 0.2 g; Molecular weight = 58.08  
92 g/mol; Mass of compound per cotton piece = 1.1 ug

93 Total surface area = 0.2 g  $\times$  0.32 m<sup>2</sup>/g = 0.064 m<sup>2</sup>

$$94 \text{ Total number of molecules} = \frac{1.1 \text{ ug}}{\frac{10^6 \text{ ug}}{\text{g}} \times 58.08 \text{ g/mol}} \times \frac{6.02 \times 10^{23} \text{ molecules}}{\text{mol}} = 1.25 \times 10^{16} \text{ molecules}$$

$$95 \text{ Surface coverage} = \frac{1.25 \times 10^{16} \text{ molecules}}{0.064 \text{ m}^2} \times \frac{1 \text{ m}^2}{10000 \text{ cm}^2} = 1.95 \times 10^{13} \text{ molecules/cm}^2$$

96 **S4. Long-term exposure in a Toronto apartment**

97 The desorption time series in Figure S3(A) were obtained from cloth samples deployed in the  
98 living room of a Toronto apartment from May 25 – July 27 2020, with exposure time of 2-10  
99 weeks. The deployment procedure matched that described in the main text but no concurrent  
100 gas-phase measurements were made at this location, precluding calculation of partition ratios.  
101 The cloth samples were transported to the laboratory for analysis in clean, sealed vessels that  
102 led to no artifacts, as demonstrated using field blanks. Assuming that the gas-phase  
103 concentrations were stable in the apartment during this period, the mass desorbed data in Figure  
104 S4 indicate that equilibrated amounts are largely stable from 2 to 10 weeks exposure.

105  
106 From an operational perspective, we note that the time at maximum temperature during thermal  
107 desorption was only 30 minutes for these analyses, as opposed to two hours for the data  
108 presented in the main paper. Comparing the shape of desorption time series for this shorter  
109 heating time with the corresponding long-time heating desorption time series (Figure S3(B), 1-  
110 5 day February 2021 laboratory samples used in main text, 2-hour heating at maximum  
111 temperature), the short-time heating desorption time series have captured the major part of the  
112 “complete” desorption time series. To evaluate the validity of the 30 minute data, in Figure S5  
113 we compare results from an additional set of partitioning coefficient measurements conducted  
114 with exposures from 1 to 7 days in the laboratory setting in December 2020 (open data points,  
115 30 minutes at maximum temperature) overlaid on top of the data presented in the main paper  
116 (closed data points, 2 hours at maximum temperature). Compared to the 2-hour heating  
117 desorption time series, the  $K_{CA}$  values are systematically lower when only 30 minutes time is  
118 used. Nevertheless, the relative positions of the log  $K_{CA}$  values from one species to another are  
119 steady.

120 **S5. Justification on the variability of physicochemical properties of isomers**

121 In PTR-MS detection, isomers are not differentiable and so confident identification of the  
122 identity of chemicals can be limited. However, the interpretation of the results may not be  
123 determined by accurate chemical identities, as the variabilities of physicochemical properties  
124 of isomers within homologous series is generally small. To illustrate, a collection of vapor  
125 pressure (VP) for selected carbonyls (aldehydes and ketones) and aromatic hydrocarbon  
126 isomers is presented in Table 1 below, sourced from the Stephenson and Malanowski (1987).<sup>5</sup>  
127 Log  $K_{OA}$  values are obtained from the ppLFER prediction in UFZ-LSER database.<sup>6</sup> Details of  
128 the sources can be found in Table S3.

129

130 Table S1. Saturated vapor pressure (VP) of liquid and log  $K_{OA}$  for selected isomers at 298 K.

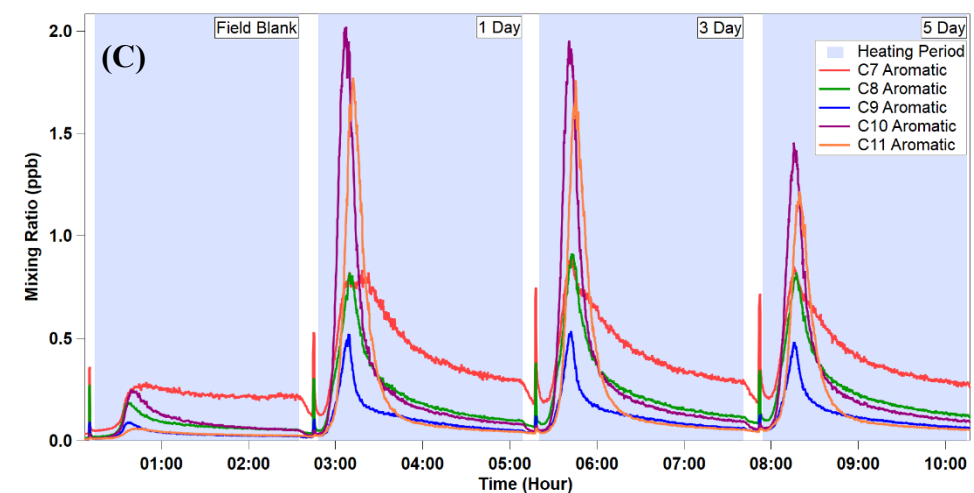
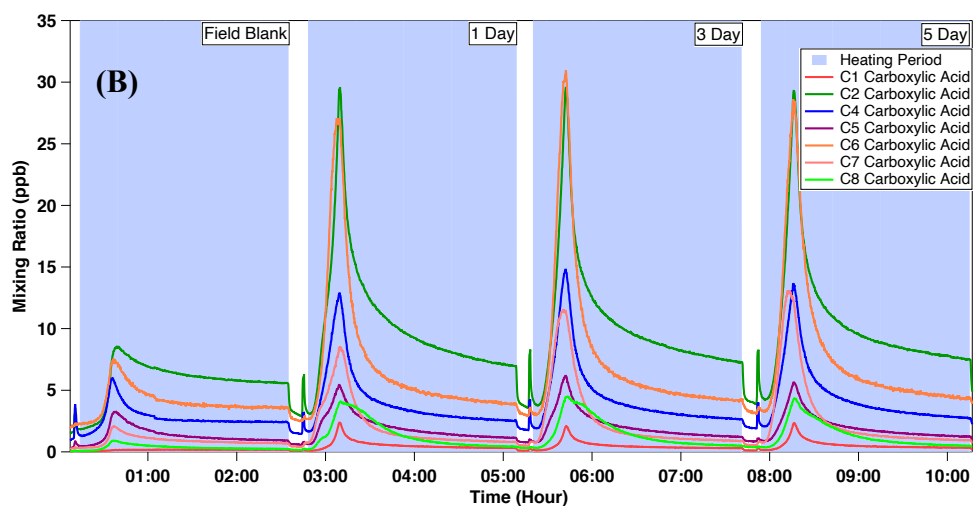
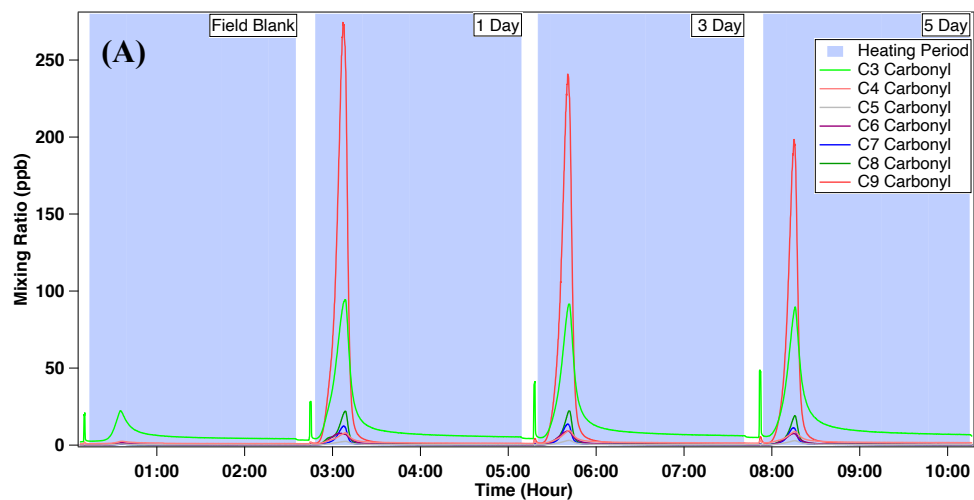
131

Formula	Identity	CAS Registry Number	Vapor Pressure at 298 K [log (VP/Pascal)]	log $K_{OA}$
C3H6O	Propanal	123-38-6	4.626	2.22
	2-Propanone (Acetone)	67-64-1	4.486	2.31
C8H16O	Octanal	124-13-0	2.503	4.62
	2,5-dimethyl-3-hexanone	1888-57-9	2.856	NA
	2,2,4-trimethyl-3-pentanone	5857-36-3	2.469	NA
	2-octanone	111-13-7	2.165	4.61
	3-octanone	106-68-3	2.453	4.60
C8H10	Ethylbenzene	100-41-4	3.098	3.67
	o-xylene	95-47-6	2.943	3.86
	m-xylene	108-38-3	3.041	3.75
	p-xylene	106-42-3	3.069	3.75

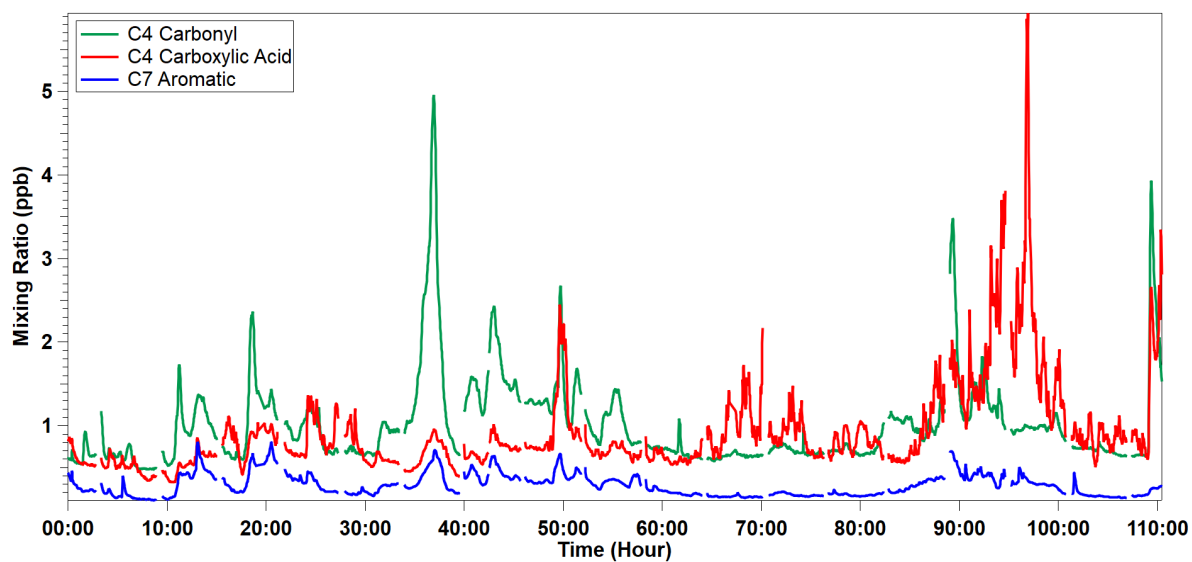
132

133 As seen from Table S1, the physical chemical properties of isomers do not vary greatly.

134 **Figure S1.** Desorption time series collected by Vocus PTR-MS to derive partition ratios ( $K_{CA}$ )  
135 for C3-9 carbonyls (A), C1,2,4-8 carboxylic acids (B), and C6-11 aromatics (C).

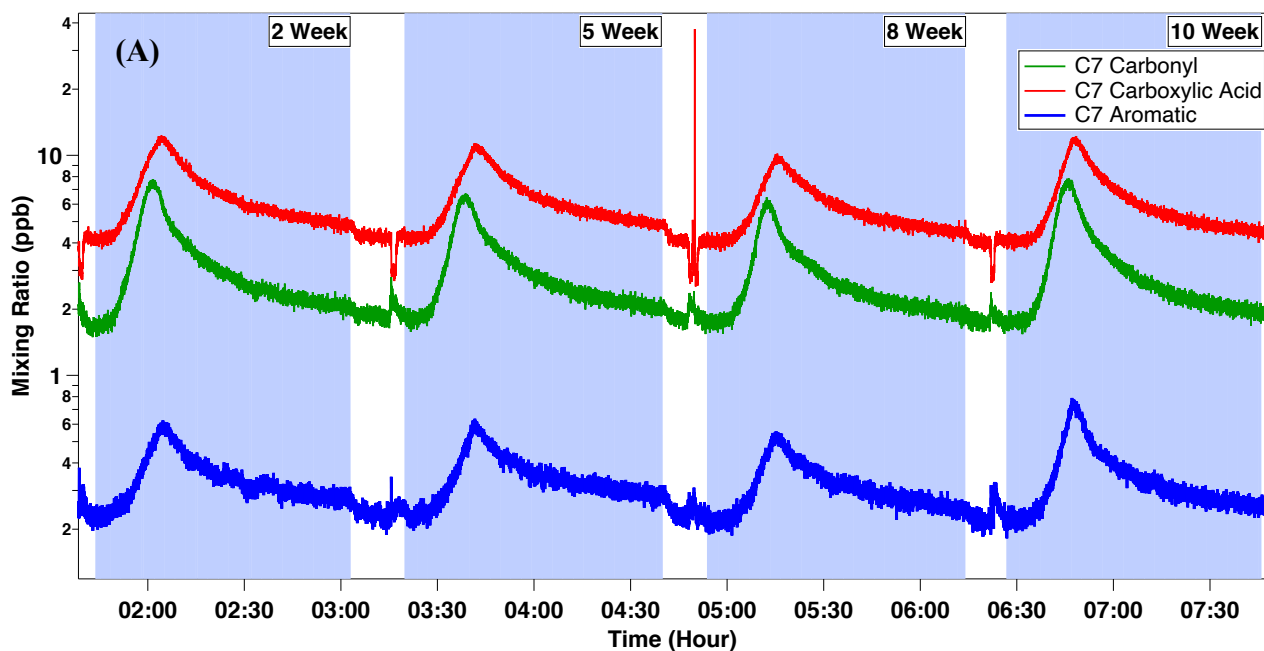


139 **Figure S2.** Real-time (5-day) ambient air signals during sample exposure period in February  
140 2021 for corresponding species shown in Figure 1. With no use of chemicals near the  
141 instrument inlet during data collection, the spikes in signal are possibly due to human presence  
142 and circulation of room air.

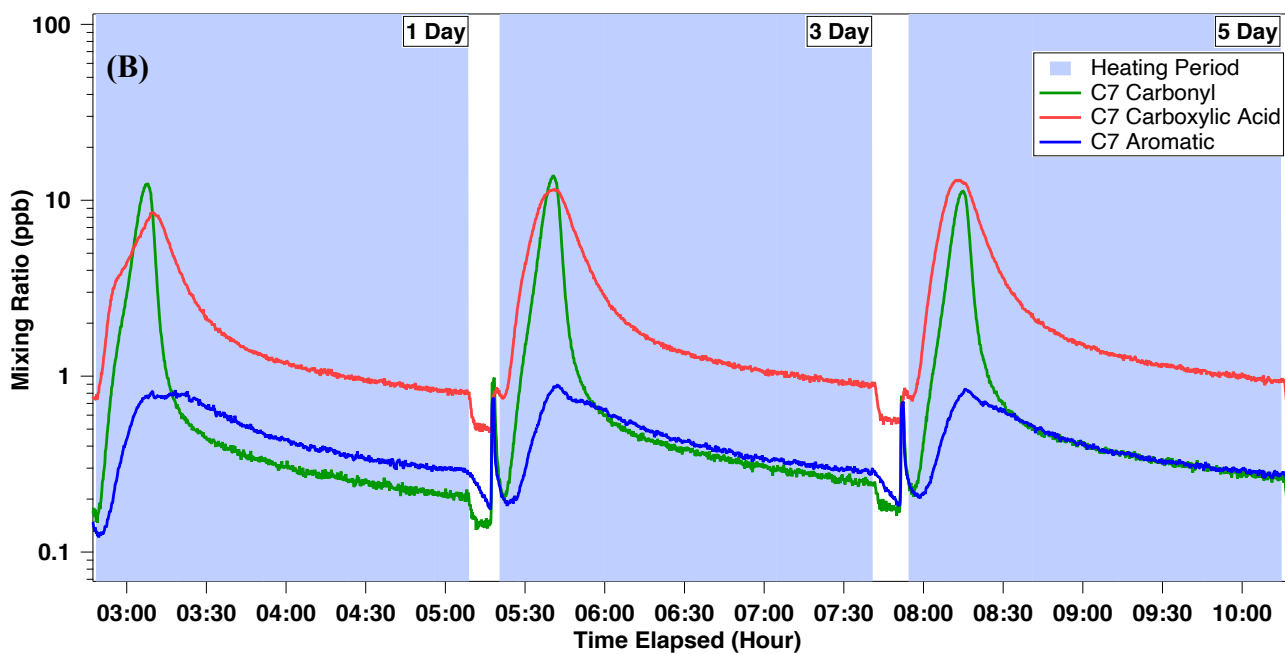


143

144 **Figure S3. (A)** Sample desorption time series of 30 minute short-time heating for cloth samples  
145 exposed in a Toronto apartment for a maximum of 10 weeks, in May to July 2020. Comparing with  
146 the corresponding desorption time series for 2-hour heating February 2021 **(B)**, this short-time  
147 heating has captured the major part of the corresponding desorption time series.

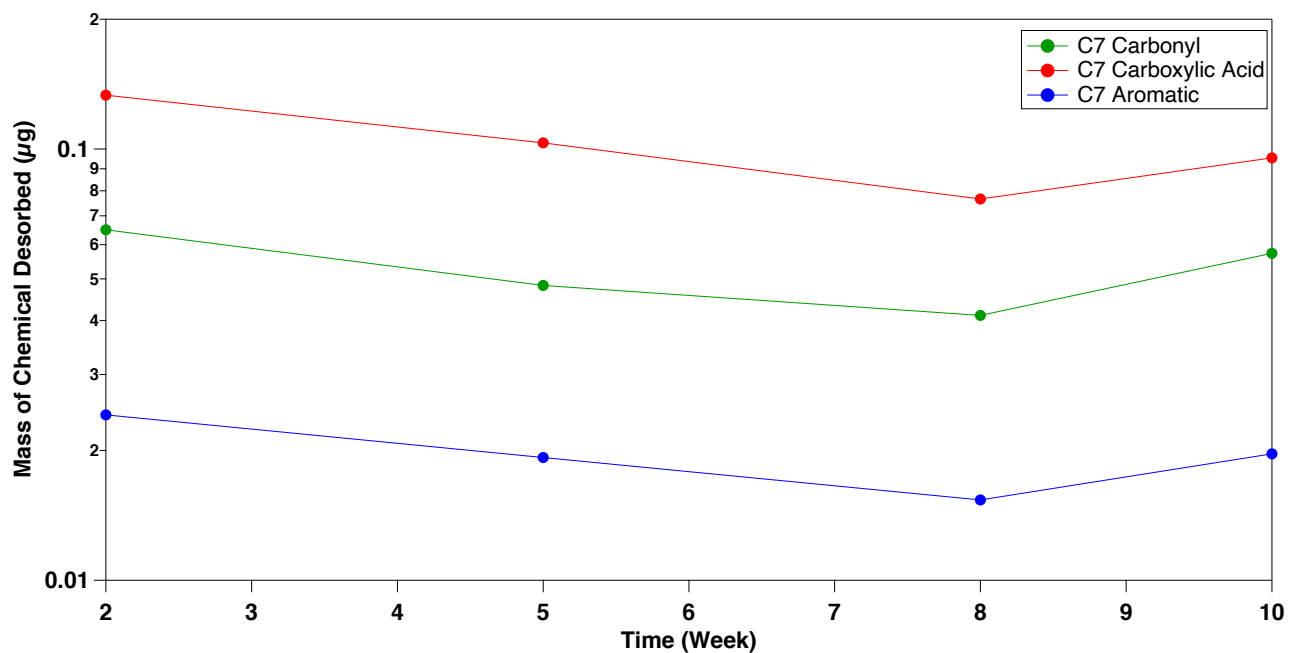


148



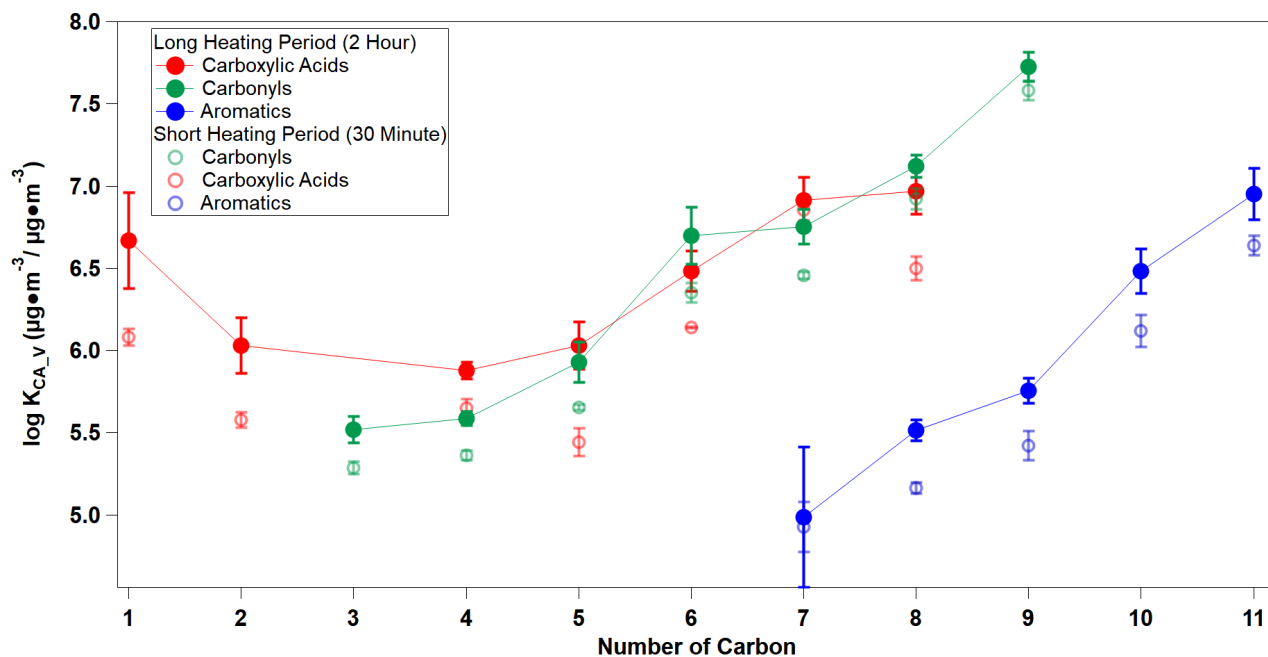
149

150 **Figure S4.** The mass desorbed ( $\mu\text{g}$ ) from samples that are exposed to apartment air as a function  
151 of exposure time, calculated from the desorption time series in **Fig. S3 (A)**. Assuming the gas-  
152 phase concentrations were stable during the deployment period, the equilibrated amounts are  
153 largely stable from 2-10 weeks exposure, i.e. cloth-air equilibrium had been reached in less than 2  
154 weeks of exposure.



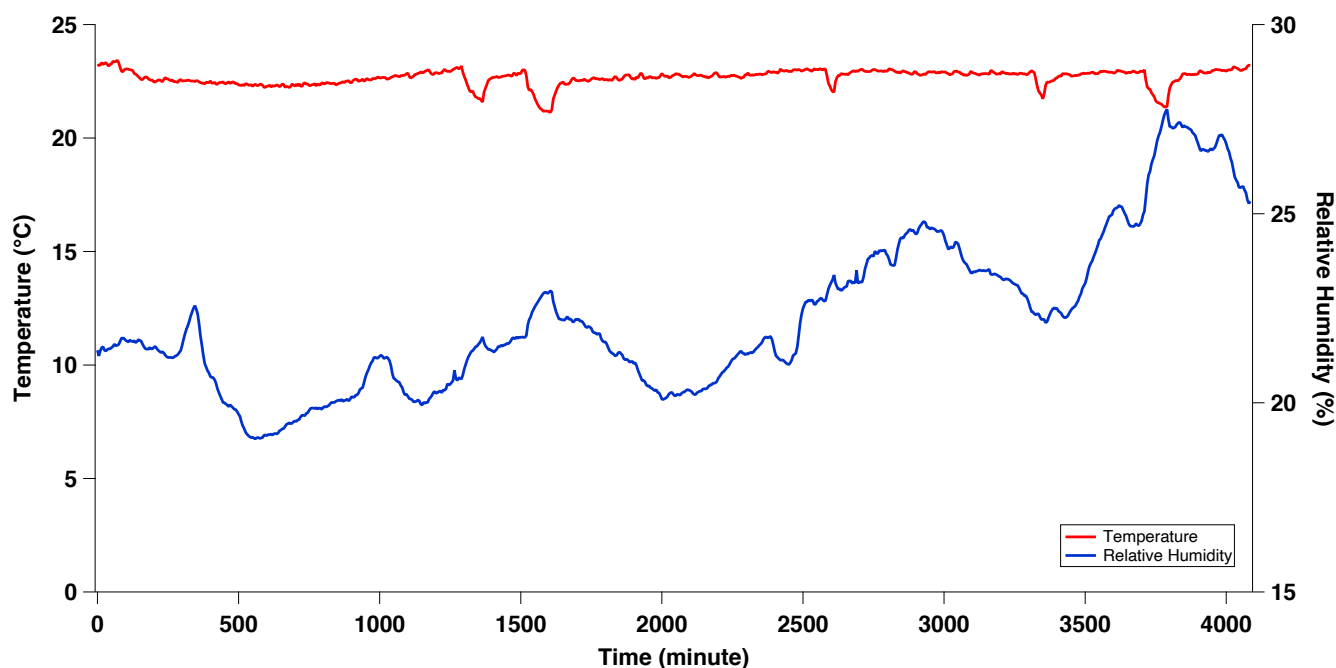
155

156 **Figure S5.** The validity of the 30-min short-time heating measurements is made via  
 157 comparison of the  $K_{CA\_V}$  values for long-time (2-hour heating; from data presented in the main  
 158 paper in December 2020 and February 2021) vs short-time (30-minute heating; from an  
 159 additional set of 1-7 day data in December 2020) thermal desorption. The  $K_{CA\_V}$  values derived  
 160 from short-time heating (open data points) are systematically lower but close to values from  
 161 long-time heating (closed data points). However, the relative positions of the log  $K_{CA\_V}$  values  
 162 from one species to another are steady.

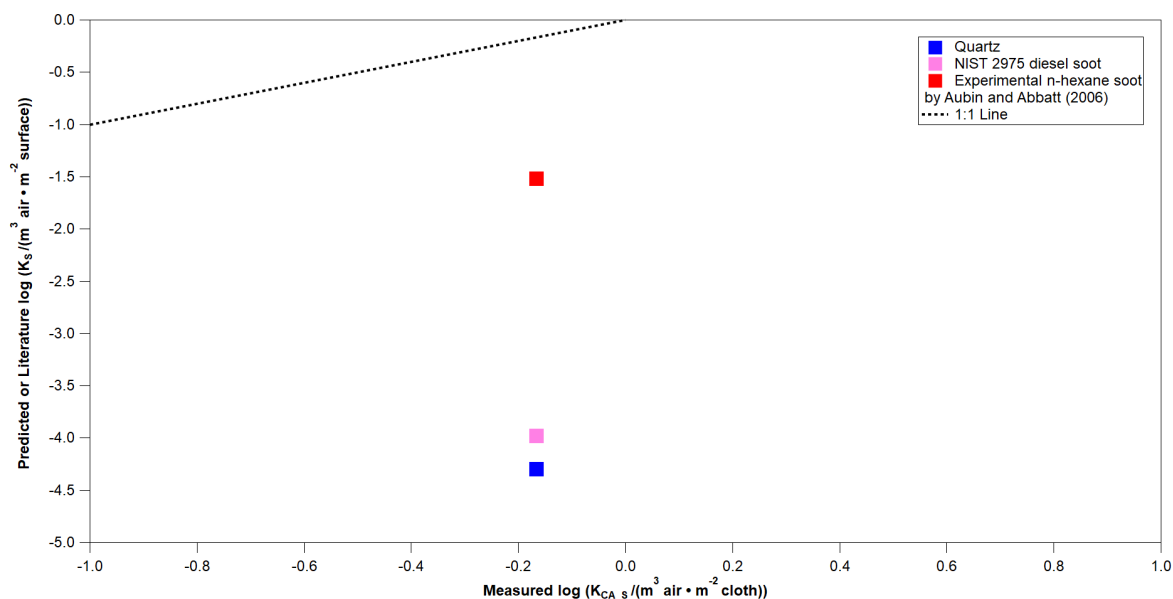


163

164 **Figure S6.** Time series of ambient temperature and relative humidity during exposure period  
 165 in February 2021. The average temperature and relative humidity remained stable at  $22.6 \pm$   
 166  $0.3$  °C and  $22.2 \pm 2.1\%$ , respectively.



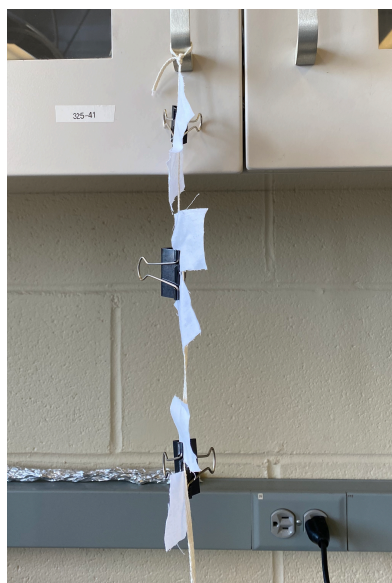
167  
 168  
 169 **Figure S7.** Surface adsorption partition ratio comparison for ethylbenzene: correlation of  
 170 measured  $\log K_{CA,S}$  values with ppLFER-predicted  $\log K_S$  for Quartz-air system at 45% RH  
 171 and NIST 2975 diesel soot – air system. The red square indicates the comparison of  
 172 ethylbenzene with Aubin and Abbatt (2016): they obtained a  $\log K_S$  of -1.522 m, the  
 173 corresponding  $\log K_{CA,S}$  is - 0.166 m in this study.



174

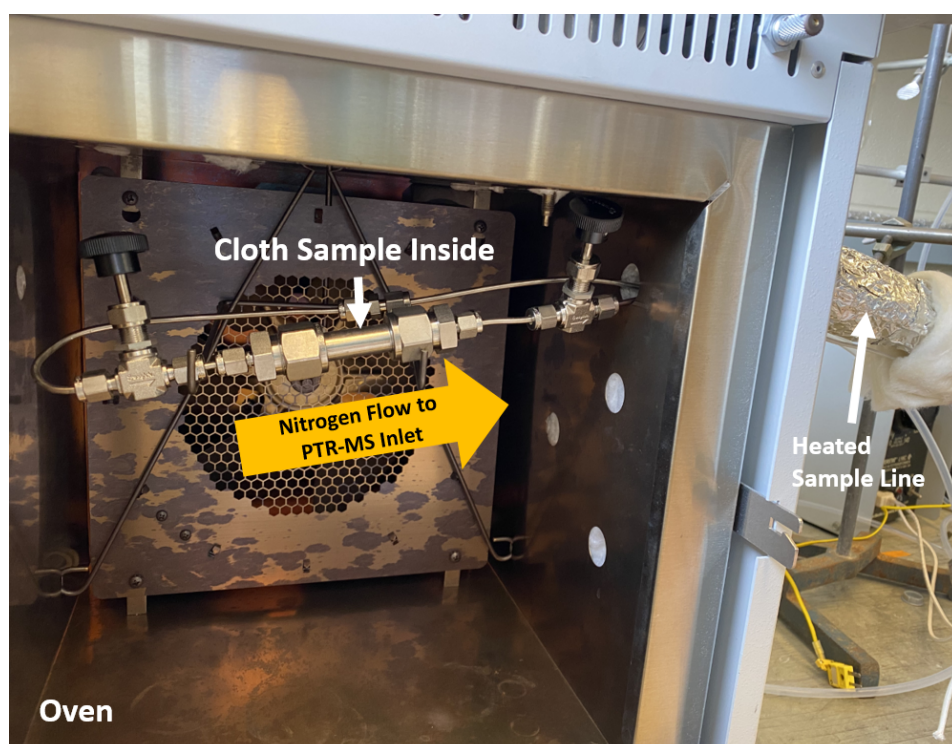
175 **Figure S8.** Illustrations for (A) Exposure set up; (B) Flow cell system.

176 (A) Cloth samples were hung vertically in the laboratory for various timed exposure periods.



177

178 (B) The stainless-steel flow cell system was situated in an old GC oven, cloth samples were  
179 placed inside the cell, one at a time for thermal desorption experiment at 135 °C. A nitrogen  
180 flow was sent through the system, and a heated Teflon sample line were used to transport  
181 desorbed signal to PTR-MS.



182

183 **Table S2.** (A) Measured sensitivity calibration factor (CF) of calibrated VOCs and predicted  
 184  $k_{\text{proton-transfer}}$  values; (B) Predicted calibration factor for all VOCs and the relevant parameters.

185 (A)

Calibrated Chemical	Parent ion fraction	Measured parent ion CF (cps/ppb)	$k_{\text{proton-transfer}}$ ( $\text{cm}^3/\text{molecule} \cdot \text{s}$ ) <sup>*4</sup>
Nonanal (C9 carbonyl)	0.13	188	$3.13 \times 10^{-9}$
Acetic acid (C2 carboxylic acid)	0.53	577	$2.2 \times 10^{-9}$
Butanoic acid (C4 carboxylic acid)	0.22	139	$2.23 \times 10^{-9}$
Hexanoic acid (C6 carboxylic acid)	0.12	53	/
Toluene (C7 aromatic)	1	1286	$2.06 \times 10^{-9}$

186 \*  $k_{\text{proton-transfer}}$  obtained from the online PTR library as described by Pagonis et al. (2019).<sup>4</sup>

187 (B)

Chemical	Assumed parent ion fraction	$k_{\text{proton-transfer}}$ ( $\text{cm}^3/\text{molecule} \cdot \text{s}$ )	Predicted parent ion CF (cps/ppb)
<b>Carbonyls</b>			
Propanal (C3)	0.13	$3.13 \times 10^{-9}$	234
Butanal (C4)	0.13	$3.17 \times 10^{-9}$	237
Pentanal (C5)	0.13	$3.02 \times 10^{-9}$	226
Hexanal (C6)	0.13	$3.05 \times 10^{-9}$	228
Heptanal (C7)	0.13	$3.06 \times 10^{-9}$	229
Octanal (C8)	0.13	$3.09 \times 10^{-9}$	231
<b>Carboxylic Acids</b>			
Formic acid (C1)	0.12	$1.92 \times 10^{-9}$	260 (*assume 50% transmission efficiency)
Pentanoic acid(C5)	0.12	$2.34 \times 10^{-9}$	157
Heptanoic acid(C7)	0.12	$2.45 \times 10^{-9}$	165
Octanoic acid(C8)	0.12	$2.56 \times 10^{-9}$	172
<b>Aromatics Hydrocarbons</b>			
Ethylbenzene (C8)	1	$2.22 \times 10^{-9}$	1289
Propylbenzene (C9)	1	$2.37 \times 10^{-9}$	1376
Butylbenzene (C10)	1	$2.49 \times 10^{-9}$	1444
Pentamethylbenzene (C11)	1	$2.60 \times 10^{-9}$	1509

188

189 **Table S3.** Summary of the numerical values of  $K_{CA}$ , error bar  $\log K_{OA}$  values that are presented  
 190 in Figure 3 - 5.

Proposed identity	Log $K_{CA\_V}$	$\log K_{CA\_V}$ Error bar	$\log K_{CA\_S}$	$\log K_{CA\_S}$ Error bar	$\log K_{OA}^*$	Vapor Pressure [ $\log (VP/Pascal)$ ]**
<b>Carbonyls</b>						
Propanal	5.52	0.08	- 0.16	0.08	2.22	4.63
Butanal	5.58	0.04	- 0.097	0.04	2.65	4.17
Pentanal	5.93	0.12	0.25	0.12	3.20	3.33
Hexanal	6.70	0.17	1.02	0.17	3.68	3.08***
Heptanal	6.75	0.11	1.07	0.11	4.16	2.23
Octanal	7.12	0.07	1.44	0.07	4.62	2.50
Nonanal	7.72	0.09	2.04	0.09	5.08	1.92
<b>Carboxylic Acids</b>						
Formic acid	6.67	0.29	0.99	0.29	4.57	3.75
Acetic acid	6.03	0.17	0.35	0.17	4.28	3.32
Butanoic acid	5.88	0.05	0.20	0.05	5.26	2.13
Pentanoic acid	6.03	0.15	0.35	0.15	5.76	1.22
Hexanoic acid	6.48	0.12	0.80	0.12	6.28	0.75
Heptanoic acid	6.92	0.14	1.23	0.14	6.62	0.27
Octanoic acid	6.97	0.14	1.29	0.14	7.10	0.56
<b>Aromatics Hydrocarbons</b>						
Toluene	4.99	0.43	-0.70	0.43	3.25	3.58
Ethylbenzene	5.52	0.06	-0.17	0.06	3.68	3.10
n-Propylbenzene	5.76	0.08	0.075	0.08	4.09	2.65
n-Butylbenzene	6.48	0.14	0.80	0.14	4.57	2.13
Pentamethylbenzene	6.95	0.16	1.27	0.16	5.64	0.97

191 \*PP-LFER fitting coefficients from Abraham et al.<sup>7</sup> The PP-LFER equation is  $\log K_{OA} = 0.94L + 0.56S + 3.51A$   
 192  $+ 0.75B - 0.21E - 0.15$  at 25 °C where the L, S, A, B and E are defined in Abraham et al.<sup>7</sup>

193 \*\* The saturated vapor pressure values of the liquid are calculated for 298 K from the Antoine equation  $\log_{10} P =$   
 194  $A - \frac{B}{C+T}$ , where the Antoine constants A, B, C are obtained from Stephenson and Malanowski (1987).<sup>5</sup>

195 \*\*\* Antoine constants unavailable, thus the vapor pressure value at 297K is referenced from Verevkin et al. (2003).<sup>8</sup>

196

197 **Reference:**

- 198 (1) Krechmer, J.; Lopez-Hilfiker, F.; Koss, A.; Hutterli, M.; Stoermer, C.; Deming, B.;  
199 Kimmel, J.; Warneke, C.; Holzinger, R.; Jayne, J.; Worsnop, D.R.; Fuhrer, K.; Gonin,  
200 M.; de Gouw, J. Evaluation of a New Reagent-Ion Source and Focusing Ion-Molecule  
201 Reactor for Use in Proton-Transfer-Reaction Mass Spectrometry. *Anal. Chem.* **2018**,  
202 *90* (20), 12011–12018. <https://doi.org/10.1021/acs.analchem.8b02641>.
- 203 (2) Liu, Q.; Abbatt, J. P. D. Liquid Crystal Display Screens as a Source for Indoor Volatile  
204 Organic Compounds. *Proc. Natl. Acad. Sci. U. S. A.* **2021**, *118* (23).  
205 <https://doi.org/10.1073/pnas.2105067118>.
- 206 (3) Sekimoto, K.; Li, S. M.; Yuan, B.; Koss, A.; Coggon, M.; Warneke, C.; de Gouw, J.  
207 Calculation of the Sensitivity of Proton-Transfer-Reaction Mass Spectrometry (PTR-  
208 MS) for Organic Trace Gases Using Molecular Properties. *Int. J. Mass Spectrom.*  
209 **2017**, *421* (1), 71–94. <https://doi.org/10.1016/j.ijms.2017.04.006>.
- 210 (4) Pagonis, D.; Sekimoto, K.; de Gouw, J. A Library of Proton-Transfer Reactions of  
211 H<sub>3</sub>O<sup>+</sup> Ions Used for Trace Gas Detection. *J. Am. Soc. Mass Spectrom.* **2019**, *30* (7),  
212 1330–1335. <https://doi.org/10.1007/s13361-019-02209-3>.
- 213 (5) Stephenson, R. M.; Malanowski, S. *Handbook of the Thermodynamics of Organic*  
214 *Compounds*, 1st ed.; Elsevier Science Publishing Co. Inc, 1987.  
215 <https://doi.org/10.1007/978-94-009-3173-2>.
- 216 (6) Ulrich, N.; Endo, S.; Brown, T. N.; Watanabe, N.; Bronner, G.; Abraham, M. H.;  
217 Goss, K. UFZ - LSER Database  
218 [https://www.ufz.de/index.php?en=31698&contentonly=1&m=0&lserd\\_data\[mvc\]=Pu](https://www.ufz.de/index.php?en=31698&contentonly=1&m=0&lserd_data[mvc]=Public/start)  
219 [blic/start](https://www.ufz.de/index.php?en=31698&contentonly=1&m=0&lserd_data[mvc]=Public/start) (accessed Jul 28, 2021).
- 220 (7) Abraham, M. H.; Smith, R. E.; Luchtefeld, R.; Boorem, A. J.; Lou, R.; Acree, W. E.  
221 Prediction of Solubility of Drugs and Other Compounds in Organic Solvents. *J.*  
222 *Pharm. Sci.* **2010**, *99* (3), 1500–1515. <https://doi.org/10.1002/jps.21922>.
- 223 (8) Verevkin, S. P.; Krasnykh, E. L.; Vasil'tsova, T. V.; Koutek, B.; Doubsky, J.; Heintz,  
224 A. Vapor Pressures and Enthalpies of Vaporization of a Series of the Linear Aliphatic  
225 Aldehydes. *Fluid Phase Equilib.* **2003**, *206* (1–2), 331–339.  
226 [https://doi.org/10.1016/S0378-3812\(03\)00035-9](https://doi.org/10.1016/S0378-3812(03)00035-9).
- 227